catalysts

MDPI

Article

Enhancing the Visible Light Photocatalytic Activity of TiO_2-Based Coatings by the Addition of Exfoliated g-C_3N_4

Ilias Papailias [1,*], Nadia Todorova [1], Tatiana Giannakopoulou [1], Niki Plakantonaki [1], Michail Vagenas [1], Panagiotis Dallas [1], George C. Anyfantis [2], Ioannis Arabatzis [2] and Christos Trapalis [1,*]

[1] Institute of Nanoscience and Nanotechnology, NCSR "Demokritos", Patriarchou Gregoriou E & 27 Neapoleos Str., 15341 Agia Paraskevi, Greece; n.todorova@inn.demokritos.gr (N.T.); t.giannakopoulou@inn.demokritos.gr (T.G.); n.plakantonaki@inn.demokritos.gr (N.P.); m.vagenas@inn.demokritos.gr (M.V.); p.dallas@inn.demokritos.gr (P.D.)

[2] NanoPhos S.A., Science and Technology Park of Lavrio, 19500 Lavrio, Greece; gc.anyfantis@gmail.com (G.C.A.); iarabatz@nanophos.com (I.A.)

* Correspondence: i.papailias@inn.demokritos.gr (I.P.); c.trapalis@inn.demokritos.gr (C.T.); Tel.: +30-210-650-3347 (I.P.); +30-210-650-3343 (C.T.)

Abstract: In the last few years, increasing interest from researchers and companies has been shown in the development of photocatalytic coatings for air purification and self-cleaning applications. In order to maintain the photocatalyst's concentration as low as possible, highly active materials and/or combinations of them are required. In this work, novel photocatalytic formulations containing g-C_3N_4/TiO_2 composites were prepared and deposited in the form of coatings on a-block substrates. The obtained photocatalytic surfaces were tested for NOx and acetaldehyde removal from model air. It was found that the addition of only 0.5 wt% g-C_3N_4 towards TiO_2 content results in over 50% increase in the photocatalytic activity under visible light irradiation in comparison to pure TiO_2 coating, while the activity under UV light was not affected. The result was related to the creation of a g-C_3N_4/TiO_2 heterojunction that improves the light absorption and the separation of photogenerated electron-hole pairs, as well as to the inhibition of TiO_2 particles' agglomeration due to the presence of g-C_3N_4 sheets.

Keywords: g-C_3N_4; TiO_2; photocatalysis; coatings; air depollution; NOx; acetaldehyde

Citation: Papailias, I.; Todorova, N.; Giannakopoulou, T.; Plakantonaki, N.; Vagenas, M.; Dallas, P.; Anyfantis, G.C.; Arabatzis, I.; Trapalis, C. Enhancing the Visible Light Photocatalytic Activity of TiO_2-Based Coatings by the Addition of Exfoliated g-C_3N_4. *Catalysts* **2024**, *14*, 333. https://doi.org/10.3390/catal14050333

Academic Editors: Roberto Fiorenza and Ekaterina A. Kozlova

Received: 28 March 2024
Revised: 1 May 2024
Accepted: 13 May 2024
Published: 20 May 2024

1. Introduction

The effect of outdoor and indoor pollutants on human health and the environment has been a matter of increasing importance during the last decades and therefore stricter legislations regarding emissions have been continuously applied. Among the most common pollutants, nitrogen oxides (NOx) [1,2], volatile organic compounds (VOCs) [3,4], and microorganisms [5,6] have been confirmed as significantly dangerous. Continuous exposure to them can cause serious respiratory problems, while at high concentrations they are considered particularly toxic. Construction materials in buildings are directly and constantly exposed to these kinds of pollutants [7], especially in enclosed spaces (such as workplaces, tunnels, underground parking, etc.) where a great accumulation of pollutants can occur. Importantly, these spaces' surfaces can serve as large workable sites where the pollutants can be decomposed on. Thus, the research community is focusing on developing techniques and materials to utilize these surfaces for efficient air purification. In this direction, semiconductor photocatalysis is increasingly attracting the attention of researchers and companies since it is regarded as a green and viable technology that is efficient under normal ambient conditions [8]. After a photocatalyst is irradiated with UV or visible light, the generated electron-hole (e^-–h^+) pairs are separated and can react with adsorbed water and/or oxygen from the atmosphere to form reactive oxygen species (ROS). Then, the ROS may react with the organic or inorganic molecules present on the surface of the

photocatalyst, thus oxidizing and/or reducing them into harmless compounds. However, the photocatalysts cannot be used in their common powder form in real-life scenarios, as without proper immobilization they would drift away from the building surface. Therefore, photocatalytic building materials are fabricated by embedding the photocatalyst in the bulk of cements, paints, etc., or by applying the photocatalyst in the form of coatings on various surfaces [9] with the latter gaining increasing attention.

Considering that the photocatalytic reactions occur on the material surface and require direct contact between the photocatalyst and the pollutants, methods such as spray coating [10,11] and dip coating [12] need to be used to uniformly apply the photocatalytic material onto the substrate surface. In addition, to maintain the transmittance or the original color of the substrate, the coating layer should be highly transparent [13]. This means that the coating has to be thin and the concentration of the photocatalyst as low as possible. Furthermore, the coating deposition on existing building surfaces should not be followed by any severe post-deposition treatment such as high-temperature calcination, irradiation, etc. Ideally, the coating should be deposited by a one-step procedure at normal conditions (temperature and pressure) to have long-lasting bonding with the building surface and facile maintenance [14].

Titanium dioxide (TiO_2)-based coatings have been studied and used for air purification and self-cleaning applications [14–17]. Undoubtedly, TiO_2 is currently the most used photocatalyst in photocatalytic construction materials due to its high chemical stability and relatively low price [18,19]. Nonetheless, TiO_2 effectiveness is limited by its UV responsiveness owing to its wide band gap (E_g = 3.2 eV) and fast e^-–h^+ recombination caused by the high density of trap states [20,21]. Specifically, for the air depollution from NOx (NO and NO_2) gases, novel photocatalysts are searched for in order to tackle the main disadvantages of the TiO_2, i.e., UV sensitization and substantial release of toxic NO_2 product. Other metal oxides [22,23], inorganic substances like Ag_3PO_4 [24], and organic polymers like g-C_3N_4 [25,26] alone or in the form of composites have been reported as very efficient photocatalytic materials owing to their visible light sensitization and/or low emission of NO_2.

Amongst the newly developed materials, graphitic carbon nitride (g-C_3N_4) has emerged as a non-toxic, visible-light-driven (E_g = 2.7 eV) photocatalyst with exceptional optical properties and stability [27]. Over the past decade, g-C_3N_4 has been studied for renewable energy utilization [28] and environmental depollution. g-C_3N_4 has been proven promising for use in construction materials and coatings [29,30]; however, the expected wide practical application of the g-C_3N_4 photocatalyst has not been reached yet, neither as powder nor in the form of a coating.

While g-C_3N_4/TiO_2 photocatalytic powders have been extensively investigated, g-C_3N_4/TiO_2 in the form of a coating is still poorly explored. Some reports on solar fuel photocatalytic production [31], water purification [32], and air treatment [33] can be mentioned here. Generally, the increase in the photocatalyst's amount improves the photocatalytic performance of coatings, however, their transmittance and homogeneity decrease [34]; thus, the great challenge remains on how to resolve this problem without compromising the optical and photocatalytic properties.

In this work, novel photocatalytic coatings containing g-C_3N_4/TiO_2 composites were prepared by adding small quantities of chemically exfoliated g-C_3N_4 to a commercially available TiO_2 suspension of NanoPhos S.A. [35]. The modified suspensions were then sprayed on a-block substrates and the obtained coatings were examined for outdoor and indoor air purification, specifically for photocatalytic removal of NOx and acetaldehyde pollutants under UV and visible light irradiation. The photocatalytic stability of the coatings was tested in order to evaluate their suitability for real-life applications; also, the physicochemical properties of the photocatalytic component, i.e., g-C_3N_4/TiO_2 composites in the form of powder, were examined.

2. Results and Discussion

2.1. Crystalline Structure and Chemical Composition

The XRD patterns of the obtained powder samples are presented in Figure 1. The pattern of chemically exfoliated g-C_3N_4 is also given for comparison. All powder samples showed the characteristic for TiO_2 peaks attributed to its anatase (ICDD, PDF-2 #21-1272) and rutile (ICDD, PDF-2 #21-1276) phases [36]. The patterns of the composite materials showed no distinct diffraction peaks related to the exfoliated g-C_3N_4. This can be ascribed to (i) its low content, i.e., 0.1, 0.5, 1.0, 2.0, and 5 wt% towards the TiO_2; (ii) its low crystallinity due to the performed chemical exfoliation; and (iii) to the fact that the main (002) diffraction peak of g-C_3N_4 at 27.8°—corresponding to the interlayer stacking of aromatic rings with a distance of d = 0.32 nm [27]—overlaps with the (110) diffraction peak of the rutile phase at 27.4° [37].

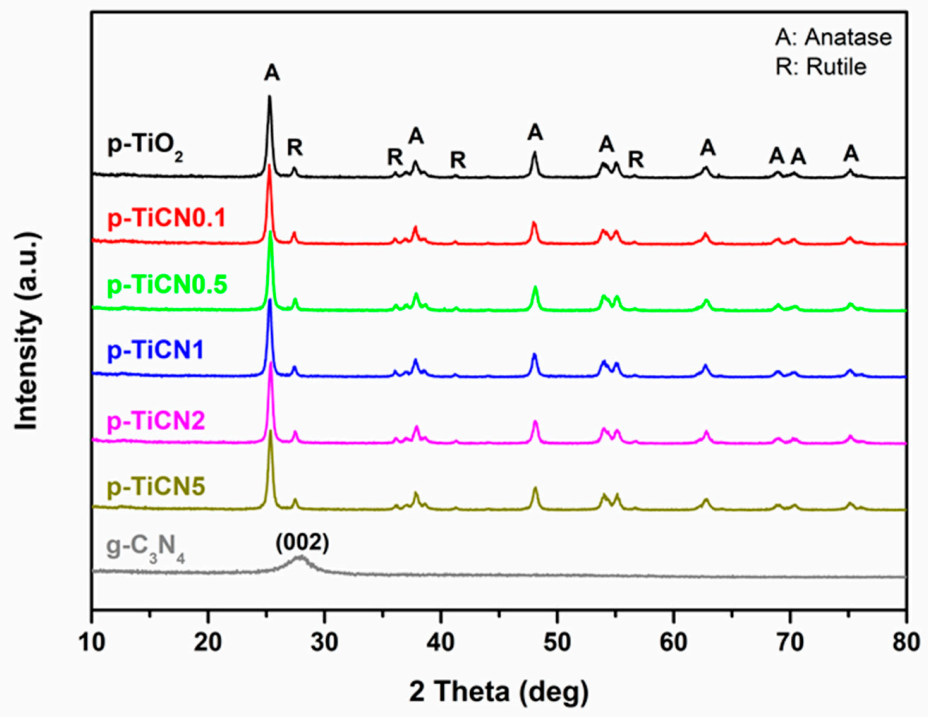

Figure 1. XRD patterns of the composite g-C_3N_4/TiO_2 powder samples and the pure TiO_2 and exfoliated g-C_3N_4.

The presence of the g-C_3N_4 in the composites was revealed by the FT-IR spectra shown in Figure 2. Specifically, the peaks between 1230 and 1630 cm^{-1} are associated with the characteristic stretching of C-N heterocycles including trigonal N-$(C)_3$ and bridging H-N-$(C)_2$ units [38,39]. Notably, the peaks become more prominent with the increase in the g-C_3N_4 concentration in the composites. Also, the broad peak from 400 to 700 cm^{-1} is attributed to the Ti-O stretching and Ti-O-Ti bridging stretching modes of TiO_2 [40], thus confirming the presence of both components of the g-C_3N_4/TiO_2 heterostructures. The observed broad peaks in the region from 3000 to 3500 cm^{-1} are attributed to N-H and O-H bonds originating from residual amino groups of the melamine precursor [41] and surface adsorbed water [42], respectively.

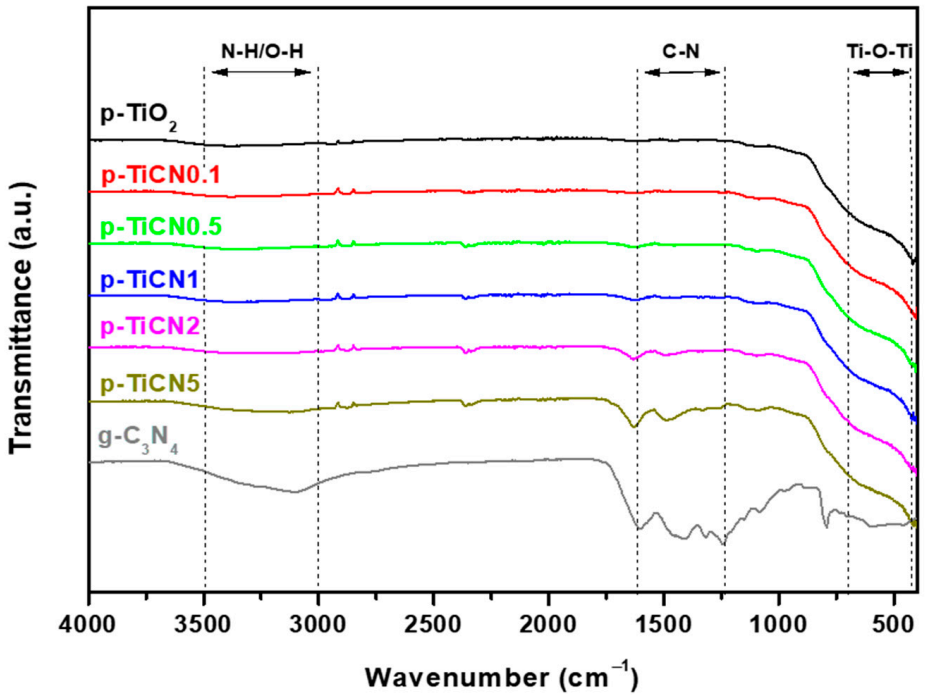

Figure 2. FT-IR spectra of the composite g-C_3N_4/TiO_2 powder samples and the pure TiO_2 and exfoliated g-C_3N_4.

2.2. Surface Area and Morphology

The liquid N_2 adsorption–desorption isotherms and the pore size distribution of the powder samples are shown in Figure 3a,b, correspondingly. All materials demonstrated characteristic hysteresis loops of type IV isotherms typical for mesoporous materials [43]. Regarding the pure components, the sample p-TiO_2 showed a specific surface area (SSA) of 48.2 m^2/g, while the exfoliated g-C_3N_4 exhibited a significantly higher SSA of 99.3 m^2/g. The g-C_3N_4/TiO_2 heterostructures exhibited SSA close to this of p-TiO_2, which slightly increases with the increase in the g-C_3N_4 content. Namely, samples p-TiCN0.1, p-TiCN0.5, p-TiCN1, p-TiCN2, and p-TiCN5 showed SSA of 48.4, 48.6, 48.9, 49.1, and 49.2 m^2/g, respectively. The materials demonstrated similar pore size distribution with a broad peak at ~180 Å (radius 18 nm) typical for the commercial P25 TiO_2 [44,45]. The peak is indicative of small and large mesopores that correspond to pores within individual nanoparticles and spaces between the formed agglomerates, respectively [46]. The exfoliated g-C_3N_4 exhibited wider pore size distribution, which can be related to its layered structure.

In Figure 4, two typical SEM images of the samples p-TiO_2 and p-TiCN5 are presented. For sample p-TiO_2, the characteristic morphology of TiO_2 particles forming large agglomerates can be observed. In sample p-TiCN5, the lamellar sheets of exfoliated g-C_3N_4 can also be seen intermingled with the TiO_2 agglomerates. In this case, the TiO_2 agglomerates appear to be smaller in size. This is a key finding since the g-C_3N_4 sheets seem to prevent the excessive agglomeration of TiO_2 particles. This is expected to play an important role in the overall photocatalytic activity by improving the homogeneity of the prepared formulation suspension and the deposited on the a-block photocatalytic coating.

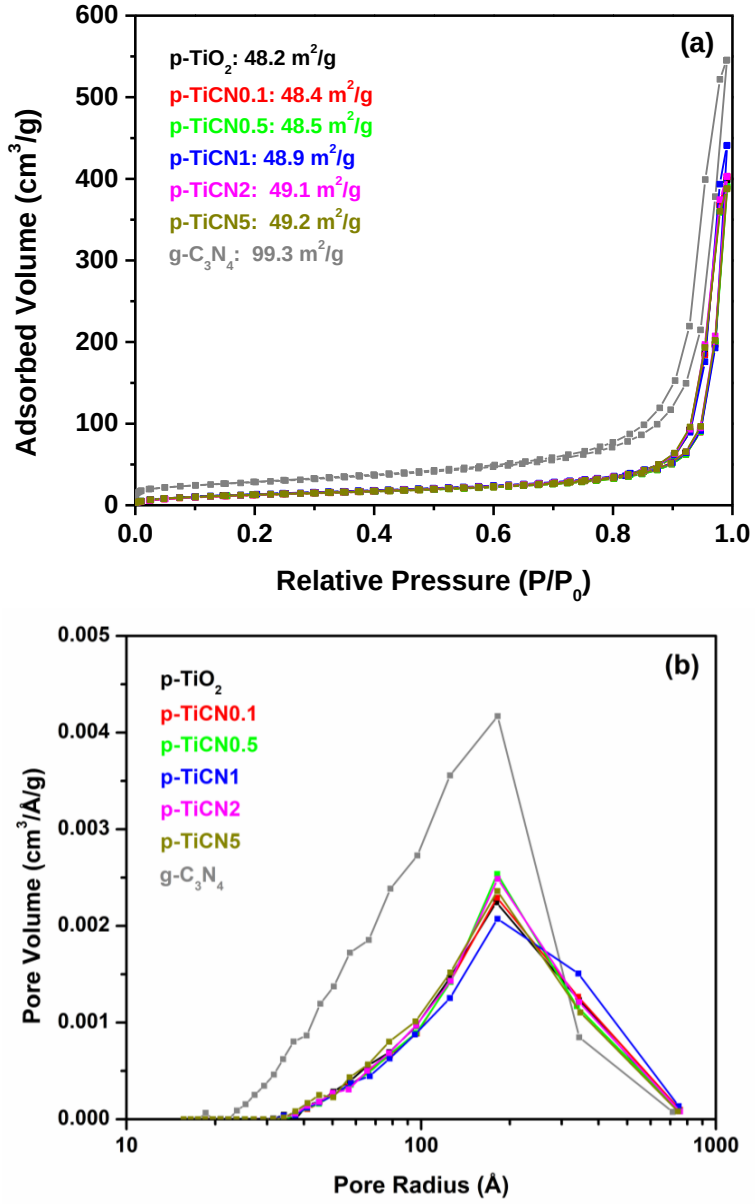

Figure 3. Liquid N_2 adsorption–desorption isotherms (**a**) and pore size distribution curves (**b**) of the powder samples.

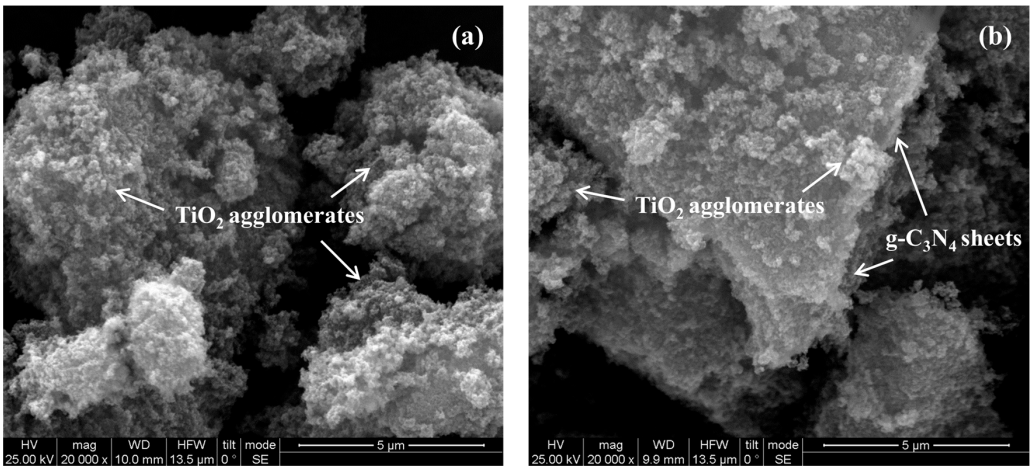

Figure 4. SEM images of powder samples p-TiO_2 (**a**) and p-TiCN5 (**b**).

2.3. Light Absorbance and Band Gap Estimation

The measured diffuse reflectance spectra (R) of the powder samples, as well as the spectrum of g-C_3N_4, are shown in Figure 5a. It is evident that the g-C_3N_4 exhibited absorbance in the visible region (between 390 and 420 nm), while the p-TiO_2 and all the composite g-C_3N_4/TiO_2 samples have similar spectra, with the main absorbance positioned between 360 and 400 nm. By utilizing the Kubelka–Munk functions $F = (1 - R)^2/2R$, the corresponding absorption functions $(F \times E)^n = f(E)$ were constructed, as depicted in Figure 5b. The two semiconductors are considered to possess an indirect band gap, and to that end, $n = 1/2$ was used. The band gap energy (E_g) of the materials was estimated by extrapolation of the linear part of the absorption functions to the *x*-axis that is the photon energy in eV [47]. It can be seen that the E_g of the g-C_3N_4 is 2.98 eV due to its exfoliated nature, while the E_g of the p-TiO_2 (3.05 eV) and all the composite g-C_3N_4/TiO_2 samples are similar (3.02–3.03 eV). The results prove that the addition of g-C_3N_4 in low concentrations does not significantly affect the E_g of the materials.

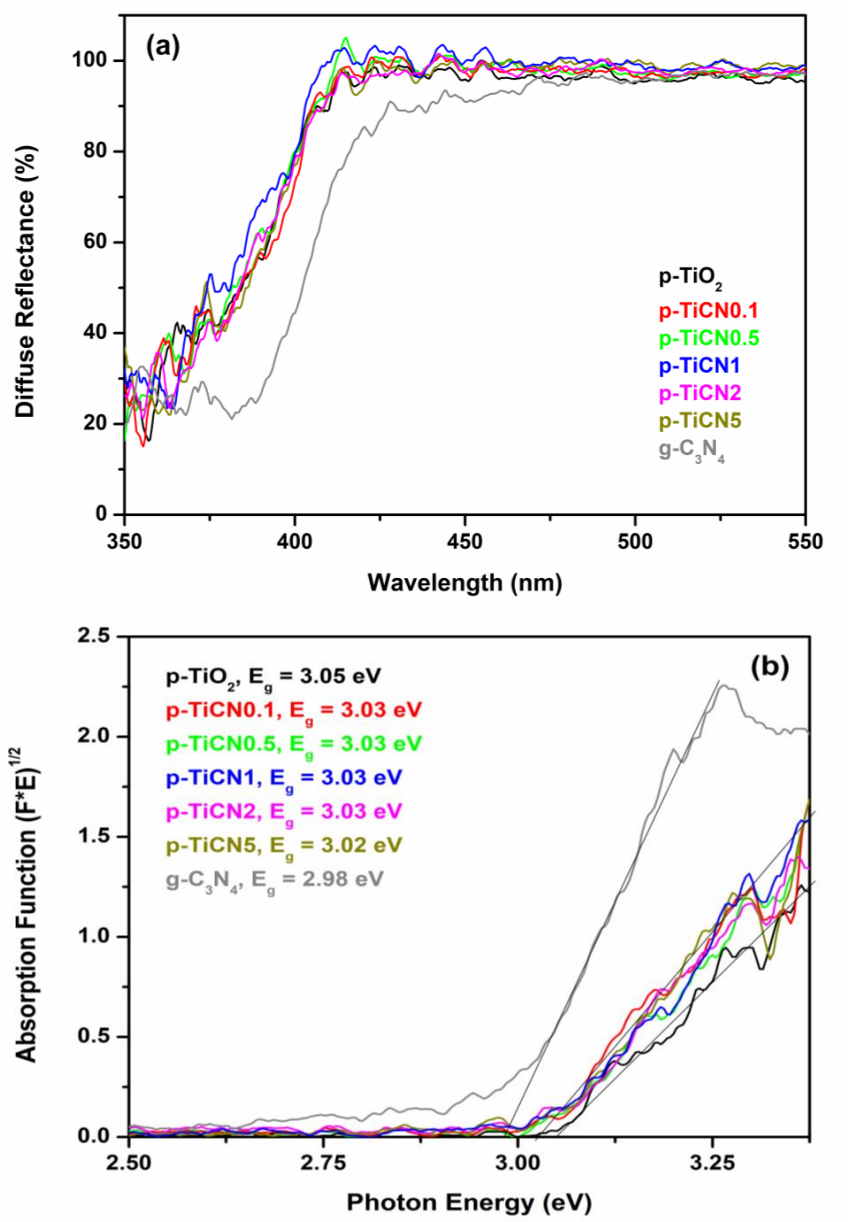

Figure 5. UV–Vis diffuse reflectance spectra (**a**) and plots of $(F \times E)^{1/2}$ vs. photon energy (**b**) of the powder samples.

2.4. Photocatalytic Activity

The variation in the gases' (NO, NO_2, and NOx) concentrations over the deposited photocatalytic coatings under dark and during light irradiation can be seen in the recorded experimental concentration curves in Figure S1. In Figure 6, the calculated changes in the gas concentrations, i.e., the decrease in the NO concentration, the increase in the NO_2 concentration, and the total decrease in the NOx concentration in the air with regard to their initial concentrations (C_{NO} = 1 ppm, C_{NO2} = 0 ppm, and C_{NOx} = 1 ppm) are presented. Under UV light irradiation (Figure 6a), all coatings showed comparable photocatalytic activity with a slightly better performance of the coating with 0.5 wt% g-C_3N_4 (sample c-TiCN0.5) achieving 48% NOx removal. However, under visible light irradiation (Figure 6b), the addition of g-C_3N_4 led to significantly enhanced activity of the coatings. The coating with 1 wt% g-C_3N_4 (sample c-TiCN1) reached 12% total NOx removal, which is 4.5% higher than the coating with pure TiO_2 (sample c-TiO_2). This increase designates the important contribution of g-C_3N_4 in broadening the light response from UV to the visible light region [37], which is essential for the real-life application of the photocatalyst.

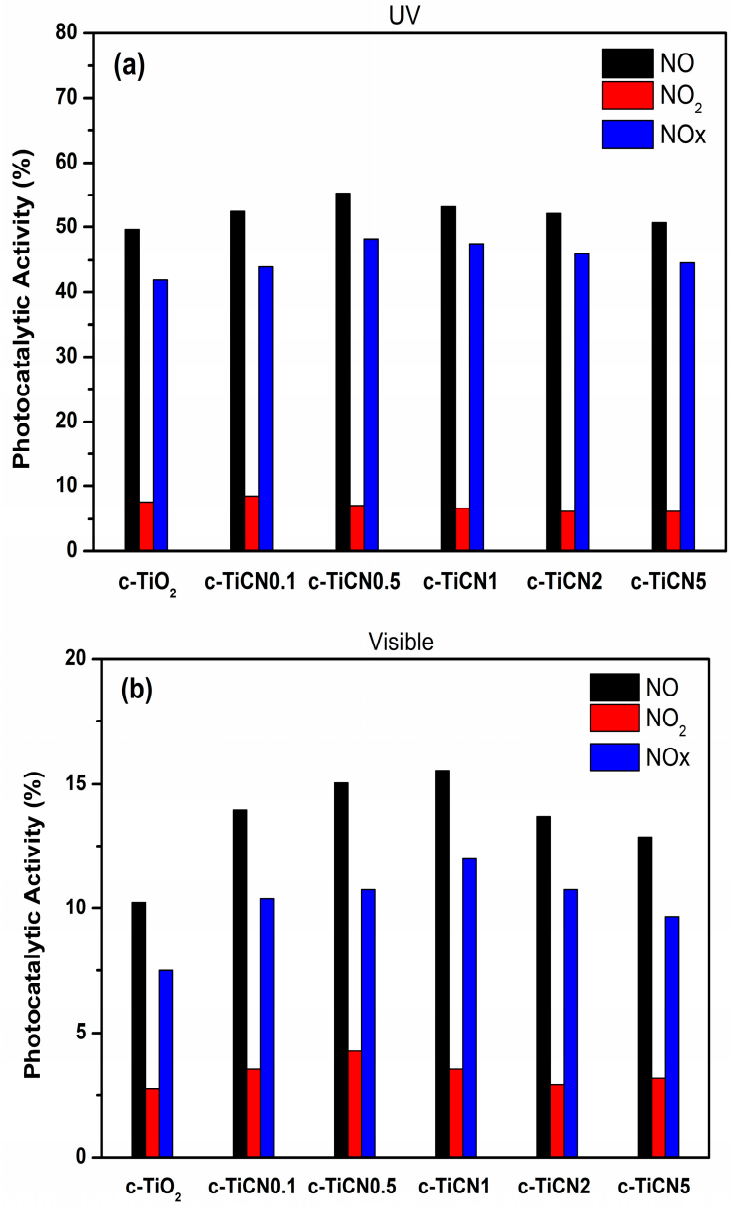

Figure 6. Photocatalytic activity of the coatings for NOx removal under UV (**a**) and visible light (**b**) irradiation.

The results for the photocatalytic acetaldehyde oxidation by the coatings under UV and visible light irradiation are presented in Figure 7, while the recorded experimental concentration curves can be seen in Figures S2 and S3. It can be observed that the sample c-TiCN0.5 exhibited the best photocatalytic activity under both UV and visible light irradiation, reaching 57% and 7.5% acetaldehyde removal, respectively. Again, the difference was more prominent under visible light where the addition of 0.5 wt% g-C_3N_4 (sample c-TiCN0.5) led to ~4% higher removal than the coating with pure c-TiO_2 (sample c-TiO_2).

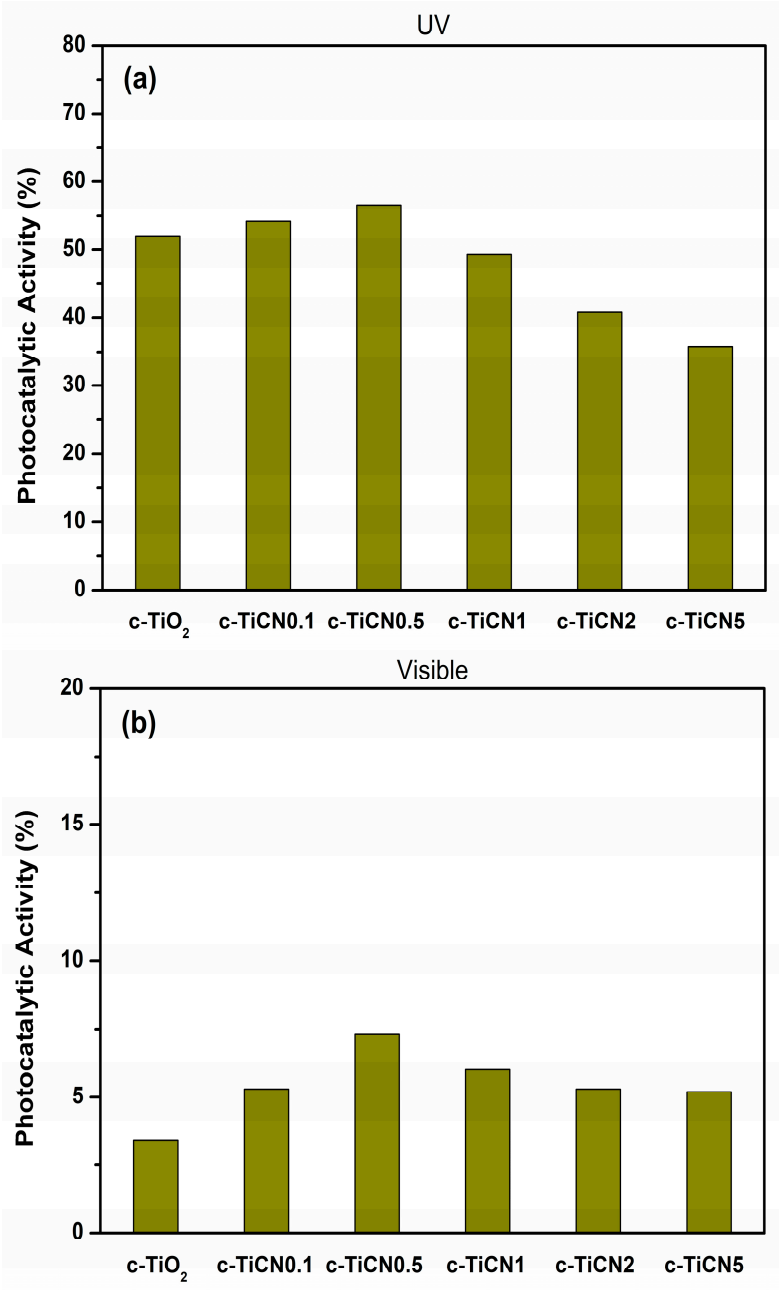

Figure 7. Photocatalytic activity of the coatings for acetaldehyde oxidation under UV (**a**) and visible light (**b**) irradiation.

In the present study, it is shown that the addition of small quantities of g-C_3N_4 to TiO_2-based formulations improves significantly the activity under visible light irradiation. Notably, major physicochemical properties influencing the photocatalytic efficiency, i.e., SSA and porosity, as well as light absorbance and width of the band gap were only slightly affected by the addition of g-C_3N_4. We would like to emphasize that the increased

photocatalytic activity can be attributed to two factors: (i) the creation of a g-C_3N_4/TiO_2 heterojunction that enhances the charge (e^- and h^+) separation; and (ii) the reduced agglomeration of the TiO_2 nanoparticles.

More specifically, the coupling between g-C_3N_4 and TiO_2 (P25) investigated in our previous work [48] revealed that the positions of the band gap's edges of the two semiconductors in the energy scale favor the formation of a heterojunction with band alignment type II. Then, taking into account the potentials for ·OH and $\cdot O_2$ radicals' formation, the most likely charge transfer mechanism is the Z-scheme [49,50], which facilitates the charge separation and reduces the recombination rate of photogenerated e^-–h^+ pairs [51–53]. It should be noted here that, as it comprises two TiO_2 phases (anatase and rutile), the P25 photocatalyst possesses its own charge separation mechanism [54,55], which results in enhanced formation of ·OH radicals on the nanoparticles' surface. Through the Z-scheme, the g-C_3N_4 component provides an additional pathway for the e^- generated in the conduction band of the TiO_2 component (CB_{TiO2}) towards its valence band ($VB_{g\text{-}C3N4}$) and finally to its conduction band ($CB_{g\text{-}C3N4}$). Thus, the charge separation in the g-C_3N_4/TiO_2 heterojunction and the formation of ·OH radicals on the composites' surface are further enhanced. In relation to this, our previous EPR results on the formation of reactive oxygen species in g-C_3N_4/TiO_2 systems with various ratios [56] also demonstrated that ·OH radicals are predominately formed in TiO_2-rich systems under visible light irradiation. Considering also that NOx and acetaldehyde oxidation mechanisms are highly dependent on ·OH radicals, the enhanced photocatalytic removal of NOx and acetaldehyde recorded in this study can be attributed to the favorable charge transfer pathways and separation in the g-C_3N_4/TO_2 heterostructures with low g-C_3N_4 content in comparison with pure p-TiO_2.

The reduced agglomeration of the TiO_2 nanoparticles—and therefore the improved homogeneity of the photocatalytic material in the formulation suspension—leads to the uniform distribution and better exposure of photocatalyst on the coated surfaces, facilitating the interaction of the gas pollutants with more photocatalytic centers. However, when the content of g-C_3N_4 exceeds a certain value (over 1 wt% towards TiO_2), the activity of the photocatalytic coatings decreases. This occurs because TiO_2 becomes covered by the g-C_3N_4 sheets, thus reducing the irradiation amount reaching the semiconductor. Also, according to [57,58], the photogenerated electron-hole pairs cannot reach the surface of the g-C_3N_4/TiO_2 composite as the g-C_3N_4 layers become recombination centers. g-C_3N_4/TiO_2 with 0.5–1.0 wt% g-C_3N_4 towards TiO_2 appeared as the optimum ratios for a suitable balance of these processes, leading to higher photocatalytic activity of the composites in comparison to the pure TiO_2 coating.

The finding that addition of only 0.5 wt% g-C_3N_4 towards TiO_2 to a well-established commercial formulation of NanoPhos S.A. results in over 50% increase in the photocatalytic activity under visible light irradiation makes the coatings suitable for immediate practical application, especially for uses where the UV light is negligible (i.e., indoor applications), while at the same time, the production cost is kept as low as possible.

Being considered for real-life application, the c-TiCN0.5 sample was subjected to weathering in order to examine its long-term stability. The results shown in Figures 8 and 9 demonstrate that after each 500-h cycle, the coating exhibited a decrease in photocatalytic activity, both for NOx and acetaldehyde removal, which is attributed to the wear and damage of the thin photocatalytic coating due to the intense weathering conditions. Critically though, even after three cycles of weathering, the coating remains active. The photocatalytic and weathering stability suggest a good adhesion of the coating to the a-block surface, which is extremely important for commercial application as no additional post-deposition treatment (usually necessary for the stabilization of coatings on a surface) is required. Considering the real-life application potential, it is established that the coating product maintains its value for approximately 18 to 36 months, which is well within the range of other commercial products.

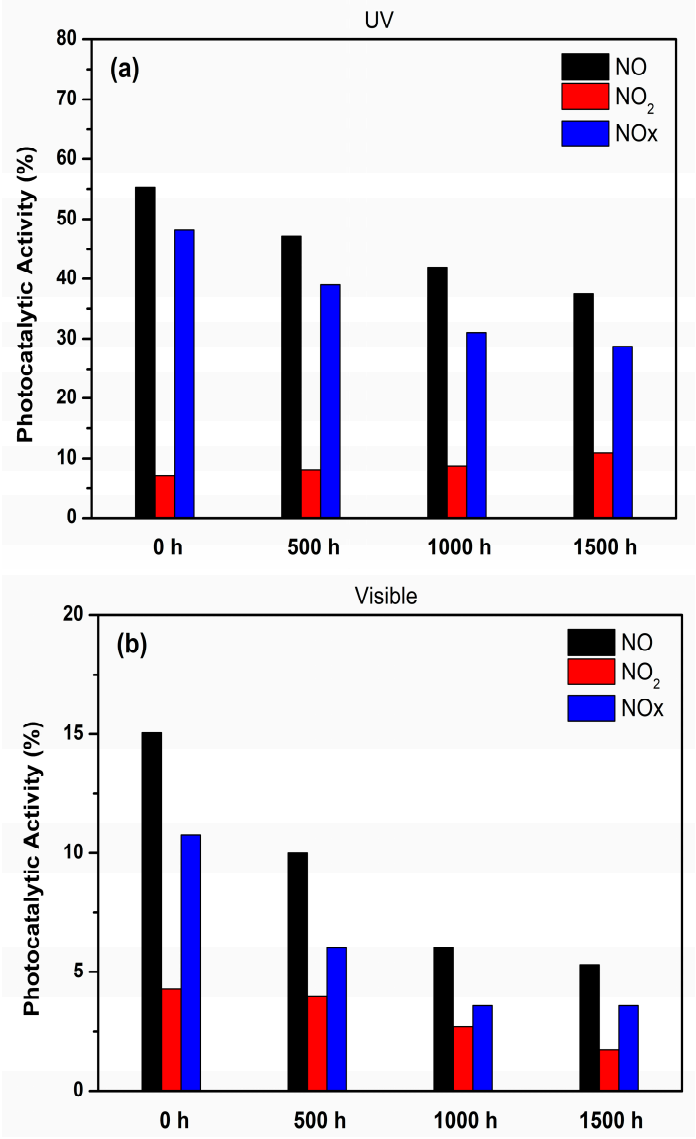

Figure 8. Photocatalytic stability of the c-TiCN0.5 coating for NOx removal under UV (**a**) and visible light (**b**) irradiation, after three consecutive weathering cycles.

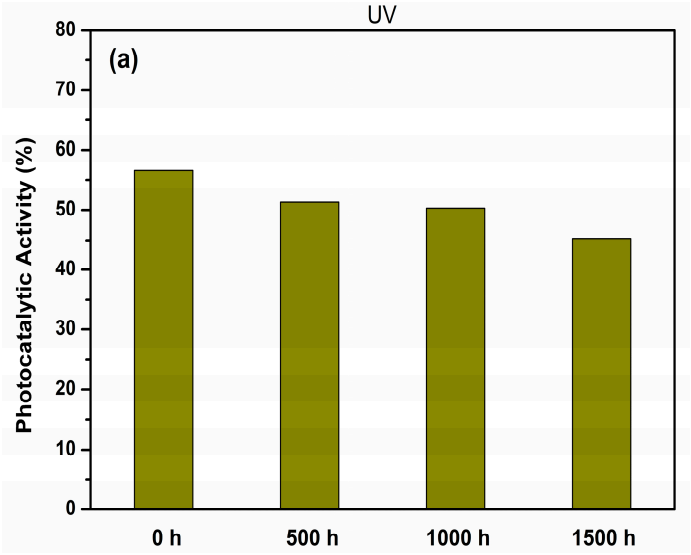

Figure 9. *Cont.*

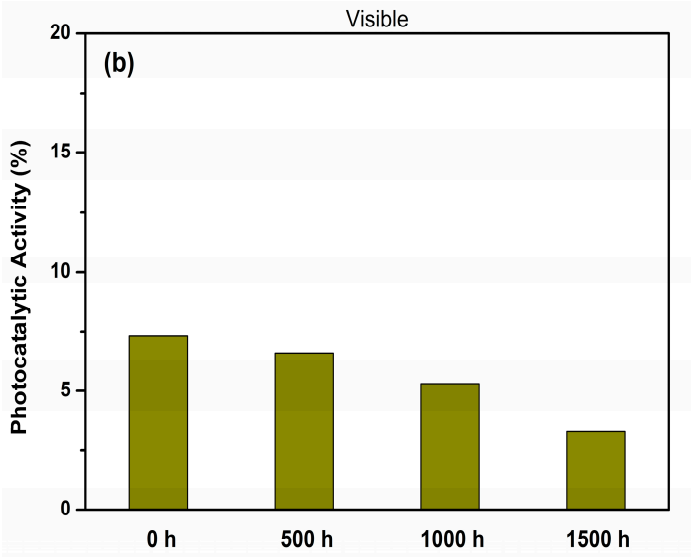

Figure 9. Photocatalytic stability of the c-TiCN0.5 coating for acetaldehyde oxidation under UV (**a**) and visible light (**b**) irradiation, after three consecutive weathering cycles.

3. Materials and Methods

3.1. Preparation of Materials and Coatings

Melamine powder was purchased from Alfa Aesar. Sulfuric acid (H_2SO_4, 98%) was purchased from Chem-Lab and isopropanol (IPA) from Sigma-Aldrich (Saint Louis, MO, USA). The chemicals were of analytical grade and were used without any further purification. The syntheses of bulk and chemically exfoliated g-C_3N_4 are described in detail in our previous work [59]. In brief, 4 g of melamine was put into an open alumina crucible and treated at 550 °C for 3 h in a tube furnace under Argon flow. The resulting yellow bulk g-C_3N_4 was ground into powder and subjected to chemical exfoliation. Namely, 0.5 g of bulk g-C_3N_4 was stirred in 8 mL concentrated H_2SO_4 for 3 h. Then, 2 mL distilled H_2O was slowly added and the suspension was poured into 100 mL distilled H_2O. After centrifugation and washing until pH 7, the remaining white powder was re-dispersed into 100 mL IPA and ultrasonicated for 1 h. Finally, the suspension was dried at 60 °C, thus obtaining exfoliated g-C_3N_4 powder.

The photocatalytic dispersions were prepared by adding a specific amount of exfoliated g-C_3N_4 in a commercially available TiO_2-containing (2 wt%) formulation provided from NanoPhos S.A. The product is patented, while coatings deposited on a glass surface were examined in our previous work [16]. In this study, the amounts of the g-C_3N_4 were calculated, taking into account the known amount of TiO_2 in the formulation suspension (Table 1). Quantities corresponding to 0.1, 0.5, 1, 2, and 5 wt% of g-C_3N_4 towards TiO_2 were added and the modified suspensions were sonicated for 15 min using a 1000 W probe-type Hielscher UIP1000hdT ultrasonic device operating at 20 kHz (Wanaque, NJ, USA). Then, the suspensions were deposited on 5 cm × 10 cm × 0.5 cm a-block substrates (coated surface 50 cm^2) using a Z-020-Tornador BLACK sprayer, (International Tool Company, Leicester, UK). The a-block is a lightweight, precast, foam-like concrete construction material with a porous surface. Its use is considered very beneficial as it insulates better than conventional bricks, while at the same time, it does not strain the building, reduces its load, and can withstand heavy constructions such as roofs. It should be mentioned that the coating was transparent and thin enough so that the coated and non-coated a-block substrates were similar in color (Figure 10). The coated substrates were left for curing at ambient conditions for at least 24 h before the photocatalytic tests. The photocatalytic coatings were named c-TiCNx, where c stands for coating and x is the wt% of g-C_3N_4 towards TiO_2.

Table 1. Experimental parameters for the preparation of the coatings: wt% of g-C_3N_4 towards TiO_2, wt% of g-C_3N_4 in the suspension, and density (d) of the suspension.

Sample	g-C_3N_4 towards TiO_2 (wt%)	g-C_3N_4 in the Suspension (wt%)	d (g/m^3)
c-TiO_2	0	0	1.41
c-TiCN0.1	0.1	0.002	1.42
c-TiCN0.5	0.5	0.010	1.42
c-TiCN1	1.0	0.020	1.42
c-TiCN2	2.0	0.040	1.42
c-TiCN5	5.0	0.100	1.43

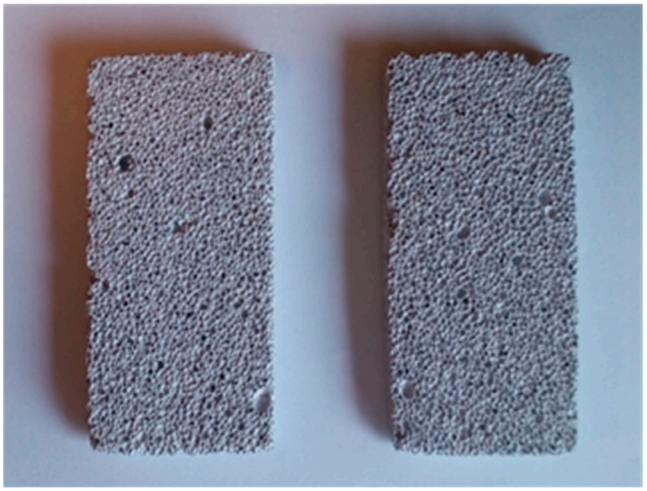

Figure 10. Coated (**left**) and non-coated (**right**) a-block substrates.

Due to the type of the substrate, physicochemical properties such as crystalline structure, specific surface area, light absorption, etc., were determined for the photocatalytic component alone. For this purpose, g-C_3N_4/TiO_2 powders were obtained by drying 5 g of the suspensions in a ventilated oven at 105 °C for 48 h. Then, the solids were collected and ground into fine powders. The samples were named p-TiCNx, where p stands for powder and x is the wt% of g-C_3N_4 towards TiO_2.

3.2. Characterization

A Siemens (Plano, TX, USA) D500 X-ray diffractometer was used for the XRD measurements. The FT-IR spectra of the materials were measured on a Nicolet (Wausau, WI, USA) iS50 spectrometer. The liquid N_2 adsorption–desorption isotherms were obtained with a Quantachrome (Boynton Beach, FL, USA) Autosorb-iQ instrument. SEM characterization was performed using an FEI (Hillsboro, OR, USA) Quanta Inspect Microscope equipped with a tungsten filament operating at 25 kV. The UV–Vis diffuse reflectance spectra were recorded by a Shimadzu (Tokyo, Japan) UV-2100 spectrophotometer using $BaSO_4$ as reference.

3.3. Photocatalytic Activity Evaluation

The photocatalytic activity of the coatings was measured for NOx removal from model gas and acetaldehyde oxidation under UV and visible light irradiation at room temperature. For the experiments, Philips (Andover, MA, USA) Cleo Compact 15 W lamps with an intensity of 10 W/m^2 and Nordex (Chicago, IL, USA) T5-8W-4000 K lamps with an intensity of 7000 lux were used, respectively.

3.3.1. NOx Removal

The photocatalytic activity of the coatings for NOx removal was evaluated using a standard procedure based on ISO/DIS 22197-1 [60]. The setup configuration and experimental

conditions are described in detail in our previous works [56,59]. Particularly, the prepared coated substrates were placed in a continuous flow reactor with dimensions 30 cm × 5 cm. The concentrations of NO, NO_2, and NOx were monitored using a Horiba APNA-370 chemiluminescence-based NOx analyzer (with a lower detectable limit of 0.0005 ppm) equipped with an O_3 lamp and a silicon photodiode sensor.

3.3.2. Acetaldehyde Oxidation

The photocatalytic activity of the coatings for acetaldehyde oxidation was evaluated using a standard procedure based on ISO/DIS 22197-2 [61]. Again, the setup configuration and experimental conditions are described in detail in our previous work [54]. The coated substrates were placed in a continuous flow reactor with dimensions 30 cm × 5 cm, while the concentration of acetaldehyde gas was monitored using a Shimadzu Tracera GC-2010 gas chromatograph equipped with a BID-2010 detector.

3.3.3. Photocatalytic Stability

The photocatalytic stability of the coatings was evaluated by performing consecutive weathering cycles using the QUV Accelerated Weathering Tester instrument by Q-Lab, which in a few days can reproduce the damage that occurs over months of outdoor exposure. To simulate outdoor weathering, the materials are subjected to alternating treatment with UV light (UVA-340 lamps at 0.71 W/m^2), condensing humidity (at 50 °C), and water spray (with rate of 5 L/min), at controlled temperatures. It is estimated that a 500 h cycle corresponds to 6–12 months of real outdoor exposure depending on the geographic location and climate characteristics. In this work, 3 cycles of 500 h were performed and after each cycle the photocatalytic activity of the coating was measured.

4. Conclusions

Novel photocatalytic coatings were prepared by adding small quantities of exfoliated g-C_3N_4 in a commercially available TiO_2 suspension and consequent deposition on construction material known as a-block. Under visible light irradiation, the coatings showed significantly increased photocatalytic activity in comparison to the commercial TiO_2-containing coatings. The result was attributed to (i) the creation of a g-C_3N_4/TiO_2 heterojunction that enhances the charge separation and reduces the recombination of the photogenerated electron-hole pairs; and (ii) the incorporation of g-C_3N_4, which inhibits the TiO_2 particles' agglomeration, thus facilitating the interaction of the gas pollutants with the photocatalytic centers. It was found that only 0.5–1.0 wt% of g-C_3N_4 towards the TiO_2 content in the suspension is required, probably due to its exfoliated nature and high specific surface area. The fact that the color of the substrate is not affected and the production cost is kept low makes the coatings very attractive for practical implementation. Additionally, the coated a-block surfaces showed significant photocatalytic and weathering stability owed to the good adhesion of the coating to the substrate surface.

Overall, the developed photocatalytic coatings are very promising for real-life applications, as they display exceptional results with negligible extra cost and without the need for additional procedures. Hopefully, this work will inspire further research and contribute to the adoption of exfoliated g-C_3N_4 for commercial and practical applications.

Supplementary Materials: The following supporting information can be downloaded at: https://www.mdpi.com/article/10.3390/catal14050333/s1. The following Figures are available: Figure S1. Experimental concentration curves of the monitored NO, NO_2, and NOx gases under UV and visible light irradiation for the photocatalytic coatings; Figure S2. Experimental concentration curves of the monitored acetaldehyde gas under UV light irradiation for the photocatalytic coatings; Figure S3. Experimental concentration curves of the monitored acetaldehyde gas under visible light irradiation for the photocatalytic coatings.

Author Contributions: Conceptualization, I.P. and C.T.; Investigation, I.P., N.T., T.G., N.P., M.V., P.D. and G.C.A.; Resources, C.T. and I.A.; Supervision, C.T.; Writing—original draft and revision, I.P. and N.T. All authors have read and agreed to the published version of the manuscript.

Funding: This research was supported by the European Union and Greek national funds through the Attica Business Plan 2014–2020, action "Research and Innovation Cooperation in the Attica Region" (project code: ATTP4-0349671).

Data Availability Statement: Data are contained within the article and Supplementary Materials.

Conflicts of Interest: Authors George C. Anyfantis and Ioannis Arabatzis were employed by the company NanoPhos S.A., Science and Technology Park of Lavrio. The remaining authors declare that the research was conducted in the absence of any commercial or financial relationships that could be construed as a potential conflict of interest.

References

1. Lira, J.D.O.B.; Padoin, N.; Vilar, V.J.; Soares, C. Photocatalytic NOx abatement: Mathematical modeling, CFD validation and reactor analysis. *J. Hazard. Mater.* **2019**, *372*, 145–153. [CrossRef] [PubMed]
2. Lasek, J.; Yu, Y.H.; Wu, J.C. Removal of NOx by photocatalytic processes. *J. Photochem. Photobiol. C* **2013**, *14*, 29–52. [CrossRef]
3. Missia, D.A.; Demetriou, E.; Michael, N.; Tolis, E.I.; Bartzis, J.G. Indoor exposure from building materials: A field study. *Atmos. Environ.* **2010**, *44*, 4388–4395. [CrossRef]
4. Kim, S.; Kim, J.A.; Kim, H.J.; Kim, S.D. Determination of formaldehyde and TVOC emission factor from woodbased composites by small chamber method. *Polym. Test.* **2006**, *25*, 605–614. [CrossRef]
5. Veltri, S.; Palermo, A.M.; De Filpo, G.; Xu, F. Subsurface treatment of TiO_2 nanoparticles for limestone: Prolonged surface photocatalytic biocidal activities. *Build. Environ.* **2019**, *149*, 655–661. [CrossRef]
6. Goffredo, G.B.; Accoroni, S.; Totti, C.; Romagnoli, T.; Valentini, L.; Munafo, P. Titanium dioxide based nanotreatments to inhibit microalgal fouling on building stone surfaces. *Build. Environ.* **2017**, *112*, 209–222. [CrossRef]
7. Wang, Z.; Gauvin, F.; Feng, P.; Brouwers, H.J.H.; Yu, Q. Self-cleaning and air purification performance of Portland cement paste with low dosages of nanodispersed TiO_2 coatings. *Constr. Build. Mater.* **2020**, *263*, 120558. [CrossRef]
8. Gartner, M.; Trapalis, C.; Todorova, N.; Giannakopoulou, T.; Dobrescu, G.; Anastasescu, M.; Osiceanu, P.; Ghita, A.; Enache, M.; Dumitru, L.; et al. Doped Sol-gel TiO_2 Films for Biological Applications. *Bull. Korean Chem. Soc.* **2008**, *29*, 1038–1042.
9. Yang, Y.; Ji, T.; Yang, Z.; Zhang, Y.; Su, W.; Wu, R.; Wu, Z. Efficiency and durability of g-C_3N_4-based coatings applied on mortar under peeling and washing trials. *Constr. Build. Mater.* **2020**, *234*, 117438. [CrossRef]
10. Faraldos, M.; Kropp, R.; Anderson, M.; Sobolev, K. Photocatalytic hydrophobic concrete coatings to combat air pollution. *Catal. Today* **2016**, *259*, 228–236. [CrossRef]
11. Lettieri, M.; Colangiuli, D.; Masieri, M.; Calia, A. Field performances of nanosized TiO_2 coated limestone for a self-cleaning building surface in an urban environment. *Build. Environ.* **2019**, *147*, 506–516. [CrossRef]
12. Li, Q.; Liu, Q.; Peng, B.; Chai, L.; Liu, H. Self-cleaning performance of TiO_2-coating cement materials prepared based on solidification/stabilization of electrolytic manganese residue. *Constr. Build. Mater.* **2016**, *106*, 236–242. [CrossRef]
13. Jiang, W.; Zong, X.; Wang, X.; Sun, Z. Transparent Coating with TiO_2 Nanorods for High-performance Photocatalytic Self-cleaning and Environmental Remediation. *Chem. Res. Chin. Univ.* **2020**, *36*, 1097–1101. [CrossRef]
14. Huang, Y.; Zhang, J.; Wang, Z.; Liu, Y.; Wang, P.; Cao, J.; Ho, W. g-C_3N_4/TiO_2 composite film in the fabrication of a photocatalytic air-purifying pavement. *Solar RRL* **2020**, *4*, 2000170. [CrossRef]
15. Todorova, N.; Giannakopoulou, T.; Pomoni, K.; Yu, J.G.; Vaimakis, T.; Trapalis, C. Photocatalytic NOx oxidation over modified ZnO/TiO_2 thin films. *Catal. Today* **2015**, *252*, 41–46. [CrossRef]
16. Arabatzis, I.; Todorova, N.; Fasaki, I.; Tsesmeli, C.; Peppas, A.; Li, W.X.; Zhao, Z. Photocatalytic, self-cleaning, antireflective coating for photovoltaic panels: Characterization and monitoring in real conditions. *Sol. Energy* **2018**, *159*, 251–259. [CrossRef]
17. Vacaroiu, C.; Enache, M.; Gartner, M.; Popescu, G.; Anastasescu, M.; Brezeanu, A.; Todorova, N.; Giannakopoulou, T.; Trapalis, C.; Dumitru, L. The effect of thermal treatment on antibacterial properties of nanostructured TiO_2(N) films illuminated with visible light. *World J. Microbiol. Biotechnol.* **2009**, *25*, 27–31. [CrossRef]
18. Zhao, J.; Yang, X. Photocatalytic oxidation for indoor air purification: A literature review. *Build. Environ.* **2003**, *38*, 645–654. [CrossRef]
19. Gauvin, F.; Caprai, V.; Yu, Q.; Brouwers, H. Effect of the morphology and pore structure of porous building materials on photocatalytic oxidation of air pollutants. *Appl. Catal. B* **2018**, *227*, 123–131. [CrossRef]
20. Osborn, D.; Hassan, M.; Asadi, S.; White, J.R. Durability quantification of TiO_2 surface coating on concrete and asphalt pavements. *J. Mater. Civ. Eng.* **2014**, *26*, 331–337. [CrossRef]
21. Guan, S.; Hao, L.; Yang, Y.; Yoshida, H.; Zhao, X.; Lu, Y. Significantly enhanced photocatalytic activity of TiO_2/TiC coatings under visible light. *J. Solid State Electrochem.* **2020**, *25*, 603–609. [CrossRef]
22. Danish, M.S.S.; Estrella, L.L.; Alemaida, I.M.A.; Lisin, A.; Moiseev, N.; Ahmadi, M.; Nazari, M.; Wali, M.; Zaheb, H.; Senjyu, T. Photocatalytic applications of metal oxides for sustainable environmental remediation. *Metals* **2021**, *11*, 80. [CrossRef]

23. Khanal, V.; Balayeva, N.O.; Günnemann, C.; Mamiyev, Z.; Dillert, R.; Bahnemann, D.W.; Subramanian, V.R. Photocatalytic NOx removal using tantalum oxide nanoparticles: A benign pathway. *Appl. Catal. B Environ.* **2021**, *291*, 119974. [CrossRef]
24. Zhang, C.; Feng, C.; Yuan, J.; Wang, Z.; Wang, Y.; Zhou, S.; Gu, P.; Li, Y. Extended construction strategies of Ag_3PO_4-based heterojunction photocatalysts for robust environmental applications. *J. Environ. Chem. Eng.* **2023**, *11*, 110705. [CrossRef]
25. Gu, Z.; Jin, M.; Wang, X.; Zhi, R.; Hou, Z.; Yang, J.; Hao, H.; Zhang, S.; Wang, X.; Zhou, E.; et al. Recent advances in g-C_3N_4-based photocatalysts for NOx removal. *Catalysts* **2023**, *13*, 192. [CrossRef]
26. Li, Y.; Sun, Y.; Ho, W.; Zhang, Y.; Huang, H.; Cai, Q.; Dong, F. Highly enhanced visible-light photocatalytic NOx purification and conversion pathway on self-structurally modified g-C_3N_4 nanosheets. *Sci. Bull.* **2018**, *63*, 609–620. [CrossRef] [PubMed]
27. Papailias, I.; Giannakopoulou, T.; Todorova, N.; Demotikali, D.; Vaimakis, T.; Trapalis, C. Effect of processing temperature on structure and photocatalytic properties of g-C_3N_4. *Appl. Surf. Sci.* **2015**, *358*, 278–286. [CrossRef]
28. Wen, J.; Xie, J.; Chen, X.; Li, X. A review on g-C_3N_4-based photocatalysts. *Appl. Surf. Sci.* **2017**, *391*, 72–123. [CrossRef]
29. Yang, Y.; Ji, T.; Su, W.; Yang, B.; Zhang, Y.; Yang, Z. Photocatalytic NOx abatement and self-cleaning performance of cementitious composites with g-C_3N_4 nanosheets under visible light. *Constr. Build. Mater.* **2019**, *225*, 120–131. [CrossRef]
30. Peng, F.; Ni, Y.; Zhou, Q.; Kou, J.; Lu, C.; Xu, Z. New g-C_3N_4 based photocatalytic cement with enhanced visible-light photocatalytic activity by constructing muscovite sheet/SnO_2 structures. *Constr. Build. Mater.* **2018**, *179*, 315–325. [CrossRef]
31. Wang, L.; Fei, X.; Zhang, L.; Yu, J.G.; Cheng, B.; Ma, Y. Solar Fuel generation over nature-inspired recyclable TiO_2/g-C_3N_4 S-scheme hierarchical thin-film photocatalyst. *J. Mater. Sci. Technol.* **2022**, *112*, 1–10. [CrossRef]
32. Wei, Z.; Liang, F.; Liu, Y.; Luo, W.; Wang, J.; Yao, W.; Zhu, Y. Photoelectrocatalytic degradation of phenol-containing wastewater by TiO_2/g-C_3N_4 hybrid heterostructure thin film. *Appl. Catal. B Environ.* **2017**, *201*, 600–606. [CrossRef]
33. Zheng, M.-W.; Wen, W.-Y.; Liu, S.-H. g-C_3N_4/TiO_2 for gas-phase formaldehyde photodegradation under visible light in the humidity control coatings. *J. Taiwan Inst. Chem. Eng.* **2024**, *154*, 105129. [CrossRef]
34. Xi, R.; Wang, Y.; Wang, X.; Lv, J.; Li, X.; Li, T.; Zhang, X.; Du, X. Ultrafine nano-TiO_2 loaded on dendritic porous silica nanoparticles for robust transparent antifogging self-cleaning nanocoatings. *Ceram. Int.* **2020**, *46*, 23651–23661. [CrossRef]
35. Available online: https://nanophos.com (accessed on 20 March 2024).
36. Tong, Z.; Yang, D.; Xiao, T.; Tian, Y.; Jiang, Z. Biomimetic fabrication of g-C_3N_4/TiO_2 nanosheets with enhanced photocatalytic activity toward organic pollutant degradation. *Chem. Eng. J.* **2015**, *260*, 117–125. [CrossRef]
37. Papailias, I.; Todorova, N.; Giannakopoulou, T.; Yu, J.G.; Dimotikali, D.; Trapalis, C. Photocatalytic activity of modified g-C_3N_4/TiO_2 nanocomposites for NOx removal. *Catal. Today* **2017**, *280*, 37–44. [CrossRef]
38. Thomas, A.; Fischer, A.; Goettmann, F.; Antonietti, M.; Mueller, J.O.; Schloegl, R.; Carlsson, J.M. Graphitic carbon nitride materials: Variation of structure and morphology and their use as metal-free catalysts. *J. Mater. Chem.* **2008**, *18*, 4893–4908. [CrossRef]
39. Dong, F.; Wu, L.W.; Sun, Y.J.; Fu, M.; Wu, Z.B.; Lee, S.C. Efficient synthesis of polymeric g-C_3N_4 layered materials as novel efficient visible light driven photocatalysts. *J. Mater. Chem.* **2011**, *21*, 15171–15174. [CrossRef]
40. Yu, J.G.; Yu, H.G.; Cheng, B.; Zhao, X.J.; Yu, J.C.; Ho, W.K. The effect of calcination temperature on the surface microstructure and photocatalytic activity of TiO_2 thin films prepared by liquid phase deposition. *J. Phys. Chem. B* **2003**, *107*, 13871–13879. [CrossRef]
41. Zhao, Y.; Liu, Z.; Chu, W.; Song, L.; Zhang, Z.; Yu, D.; Tian, Y.; Xie, S.; Sun, L. Large-scale synthesis of nitrogen-rich carbon nitride microfibers by using graphitic carbon nitride as precursor. *Adv. Mater.* **2008**, *20*, 1777–1781. [CrossRef]
42. Bojdys, M.J.; Muller, J.-O.; Antonietti, M.; Thomas, A. Ionothermal synthesis of crystalline, condensed, graphitic carbon nitride. *Chem. Eur. J.* **2008**, *14*, 8177–8182. [CrossRef] [PubMed]
43. Zhao, Z.; Sun, Y.; Luo, Q.; Dong, F.; Li, H.; Ho, W.K. Mass-controlled direct synthesis of graphene-like carbon nitride nanosheets with exceptional high visible light activity. Less is Better. *Sci. Rep.* **2015**, *5*, 14643. [CrossRef] [PubMed]
44. Fan, K.; Zhang, W.; Peng, T.; Chen, J.; Yang, F. Application of TiO_2 fusiform nanorods for dye-sensitized solar cells with significantly improved efficiency. *J. Phys. Chem. C* **2011**, *115*, 17213–17219. [CrossRef]
45. Kim, Y.E.; Byun, M.Y.; Lee, K.-Y.; Lee, M.S. Effects of chlorinated Pd precursors and preparation methods on properties and activity of Pd/TiO_2 catalysts. *RSC Adv.* **2020**, *10*, 41462–41470. [CrossRef] [PubMed]
46. Tao, T.; Glushenkov, A.M.; Chen, Q.; Hu, H.; Zhou, D.; Zhang, H.; Boese, M.; Liu, S.; Amal, R.; Chen, Y. Porous TiO_2 with a controllable bimodal pore size distribution from natural ilmenite. *CrystEngComm* **2011**, *13*, 1322–1327. [CrossRef]
47. Giannakopoulou, T.; Todorova, N.; Romanos, G.; Vaimakis, T.; Dillert, R.; Bahnemann, D.; Trapalis, C. Composite hydroxyapatite/TiO_2 materials for photocatalytic oxidation of NOx. *Mater. Sci. Eng. B* **2012**, *177*, 1046–1052. [CrossRef]
48. Giannakopoulou, T.; Papailias, I.; Todorova, N.; Boukos, N.; Liu, Y.; Yu, J.; Trapalis, C. Tailoring the energy band gap and edges' potentials of g-C_3N_4/TiO_2 composite photocatalysts for NOx removal. *Chem. Eng. J.* **2017**, *310*, 571–580. [CrossRef]
49. Afroz, K.; Moniruddin, M.; Bakranov, N.; Kudaibergenov, S.; Nuraje, N. A heterojunction strategy to improve the visible light sensitive water splitting performance of photocatalytic materials. *J. Mater. Chem. A* **2018**, *6*, 21696–21718. [CrossRef]
50. Li, J.; Zhang, M.; Li, Q.; Yang, J. Enhanced visible light activity on direct contact Z-schemeg-C_3N_4-TiO_2 photocatalyst. *Appl. Surf. Sci.* **2017**, *391*, 184–193. [CrossRef]
51. Zhou, C.; Ye, N.F.; Yan, X.H.; Wang, J.J.; Pan, J.M.; Wang, D.F.; Wang, Q.; Zu, J.X.; Cheng, X.N. Construction of hybrid Z-scheme graphitic C_3N_4/reduced TiO_2 microsphere with visible-light-driven photocatalytic activity. *J. Materiomics* **2018**, *4*, 238–246. [CrossRef]

52. Ma, J.; Wang, C.; He, H. Enhanced photocatalytic oxidation of NO over g-C_3N_4-TiO_2 under UV and visible light. *Appl. Catal. B Environ.* **2016**, *184*, 28–34. [CrossRef]
53. Lu, Z.; Zeng, L.; Song, W.; Qin, Z.; Zeng, D.; Xie, C. In situ synthesis of C-TiO_2/g-C_3N_4 heterojunction nanocomposite as highly visible light active photocatalyst originated from effective interfacial charge transfer. *Appl. Catal. B Environ.* **2017**, *202*, 489–499. [CrossRef]
54. Ohno, T.; Sarukawa, K.; Tokieda, K.; Matsumura, M. Morphology of a TiO_2 photocatalyst (Degussa, P25) consisting of anatase and rutile crystalline phase. *J. Catal.* **2001**, *203*, 82–86. [CrossRef]
55. Sun, B.; Smirniotis, P. Interaction of anatase and rutile TiO_2 particles in aqueous photooxidation. *Catal. Today* **2003**, *88*, 49–59. [CrossRef]
56. Papailias, I.; Todorova, N.; Giannakopoulou, T.; Dvoranova, D.; Brezova, V.; Dimotikali, D.; Trapalis, C. Selective removal of organic and inorganic air pollutants by adjusting the g-C_3N_4/TiO_2 ratio. *Catal. Today* **2021**, *361*, 37–42. [CrossRef]
57. Yu, J.G.; Wang, S.; Low, J.; Xiao, W. Enhanced photocatalytic performance of direct Z-scheme g-C_3N_4-TiO_2 photocatalysts for the decomposition of formaldehyde in air. *Phys. Chem. Chem. Phys.* **2013**, *15*, 16883–16890. [CrossRef] [PubMed]
58. Fagan, R.; McCormack, D.E.; Hinder, S.J.; Pillai, S.C. Photocatalytic Properties of g-C_3N_4-TiO_2 Heterojunctions under UV and Visible Light Conditions. *Materials* **2016**, *9*, 286. [CrossRef]
59. Papailias, I.; Todorova, N.; Giannakopoulou, T.; Ioannidis, N.; Boukos, N.; Athanasekou, C.P.; Dimotikali, D.; Trapalis, C. Chemical vs thermal exfoliation of g-C_3N_4 for NOx removal under visible light irradiation. *Appl. Catal. B Environ.* **2018**, *239*, 16–26. [CrossRef]
60. *ISO 22197-1*; Fine Ceramics (Advanced Ceramics, Advanced Technical Ceramics)—Test Method for Air-Purification Performance of Semiconducting Photocatalytic Materials, Part 1: Removal of Nitric Oxide. ISO: Geneva, Switzerland, 2016.
61. *ISO 22197-2*; Fine Ceramics (Advanced Ceramics, Advanced Technical Ceramics)—Test Method for Air-Purification Performance of Semiconducting Photocatalytic Materials, Part 2: Removal of Acetaldehyde. ISO: Geneva, Switzerland, 2019.